Pergamon

Int. J. Heat Mass Transfer. Vol. 40, No. 14, pp. 3407–3417, 1997

Printed in Great Britain
0017–9310/97 $17.00+0.00

PII: S0017–9310(96)00377–8

Measurement and interpretation of growth of binary droplets suspended in a water–*n*-propanol–nitrogen mixture by means of a piston-expansion-tube

T. RODEMANN and F. PETERS†
Universität GH Essen, FB 12-Strömungslehre, 45117 Essen, Germany

(*Received* 12 *August* 1996 *and in final form* 21 *October* 1996)

Abstract—We generate a cloud of monodisperse binary droplets in a piston-expansion-tube by homogeneous nucleation and subsequent growth in a supersaturated vapor. By Mie light scattering we measure the growth rate of the droplets in the radius range from 0.16 to 3 μm. We investigate the water–*n*-propanol system because the growth behavior of the pure substances is very well known from previous studies. Our model calculations are an extension of a successful unary model to the binary case in which the droplet composition is treated as a variable. The calculation starts at the nucleus, passes through the transition zone about Knudsen number one and extends to the final droplet/vapor equilibrium which is only reached when vapor depletion and heat release are taken into account. The model is in good agreement with the experimental data. © 1997 Elsevier Science Ltd.

1. INTRODUCTION

Systems consisting of small liquid droplets suspended in a gaseous phase (vapor/carrier gas mixture) occur under natural circumstances e.g. in the atmosphere as well as in technical processes, e.g. in sprays. These systems are interesting to study because their enormous surface to volume ratio involves transfer or reaction rates between phases much larger than in comparable bulk liquid systems. In a frequently encountered situation the droplets are surrounded by supersaturated vapor. Then droplet growth takes place by vapor condensation at the surface. To reach the surface the vapor diffuses through the carrier while the latent heat of condensation is conducted away from the surface. We have already completed experimental investigations on growth and evaporation of droplets consisting of a single species carried in argon or air by means of a shock tube method [1]. The species were water, methanol, *n*-propanol and *n*-hexane. With this work we proceed to condensational growth in a binary system in which two vapors condense simultaneously making a mixed droplet. This is a more complicated problem mainly because the droplet composition enters as an additional unknown which cannot yet be measured directly.

The literature provides numerous theoretical studies on condensational growth of unary droplets (see Gyarmathy [2] and Mozurkewich [3] for reviews). For a more recent fundamental paper on molecular kinetics see Barrett and Clement [4]. Kulmala [5] developed an analytical expression for the condensational growth which is valid when the droplet radius is greater than about 5 nm. Only a few publications are dealing with droplet growth in binary vapors. A growth model was proposed by Fukuta and Walter [6] for the limiting case of water vapor condensing onto water droplets containing a solute. Kaser [7] presented a closed set of equations for calculating binary droplet growth in an expansion flow of a supersonic nozzle which was never confirmed by experimental data. An analytical expression for the rate of binary droplet growth was given by Kulmala *et al.* [8], which is valid only when the sum of the vapor activities is close to unity. It may be said that a thoroughly verified and widely applicable model is still required.

A limited number of results on experimental droplet growth rates in binary mixtures is reported in the literature. Studzinski *et al.* [9, 10] observed droplet growth in water–ethanol and water–acetic acid systems for a single composition. Data on droplet growth in a water-rich mixture of water–*n*-propanol were published by Spiegel *et al.* [11]. All these experiments were conducted in the unsteady expansion fan of a shock tube using the dispersion quotient technique for droplet detection. The size range of the growing droplets was relatively small with a considerable size distribution. Studzinski *et al.* [12, 9] also proposed a simple model which, however, did not overlap with their own experimental data. Rudolf *et al.* [13] employed an expansion chamber to measure binary droplet growth. The droplets consisted of water, *n*-propanol and a heterogeneous nucleus. Along with their experiments

†Author to whom correspondence should be addressed.

NOMENCLATURE

C	kinetic factor
c_p	specific heat capacity
D	diffusion coefficient
J	nucleation rate
J^m	mass flux
J^q	heat flux
k	thermal conductivity
k_B	Boltzmann constant
L	latent heat
M	molar mass
n	refractive index
p	pressure
r	radius
R	specific gas constant
$\hat{R}$	gas constant
t	temperature (°C)
T	temperature (K)
v	molar volume
x_i	molar fraction (liquid) of comp. i
X_i	mass fraction (liquid) of comp. i
y_i	molar fraction (gas) of comp. i
Y_i	mass fraction (gas) of comp. i
x, X	without subscript means always
y, Y	n-propanol.

Greek symbols

γ	activity coefficient
Γ	dimensionless function
η	dynamic viscosity
κ	ratio of specific heats
λ	mean free path
ρ	density
σ	surface tension
ϕ	mixing function
ψ	volume fraction.

Subscripts

0	pure, bulk liquid
1	water
2	n-propanol
3	carrier gas
d	droplet
e	equilibrium
i	component i
ij	binary mixture of comp. i and j
ini	initial condition
int	edge of Knudsen interface
j	component j
nuc	nucleation
s	flat bulk surface
∞	far field.

Superscripts

l	liquid
v	vapor
σ	surface layer
*	critical nucleus
–	vapor/carrier gas mixture.

Dimensionless numbers

Kn	Knudsen-number
Pr	Prandtl-number
Sc	Schmidt-number.

they proposed a growth model based on unary models of various authors [14–16]. So far these experiments can be considered the most advanced ones despite the fact that the droplets contain a heterogeneous core.

In this work we present droplet growth curves of the binary system water–n-propanol carried in nitrogen for various compositions covering the entire mixing range. The experiments were performed in a specially designed **p**iston **ex**pansion **tube** (pex-tube), which renders it possible to generate a cloud of monodisperse droplets by homogeneous nucleation and subsequent condensational growth. The pex-tube had been used before for investigations of the growth of water droplets suspended in pure vapor [17] and for studies on binary homogeneous nucleation of water–n-propanol and water–n-butanol [18]. The radius of growing droplets is resolved as function of time in a range from 0.2 to 3 μm by means of Mie light scattering. A typical droplet number concentration is 1500 cm^{-3}. We start out with suggesting a binary model which is based on an existing unary model. We will show in the further sections that this approach is most promising.

2. MODEL

According to the situation realized in our experiments we consider monodisperse droplets evenly distributed in a mixture of vapors and carrier gas. The mixture is resting as are the suspended droplets. Their terminal velocity is too small for effective sedimentation. The spacing between droplets is sufficiently large such that coalescence becomes very unlikely on the time scale of the experiment. Hence, the droplets are independent and equal. The treatment of one stands for all. In our experimental study [1] we have already used Young's analysis [19] successfully on the growth of unary droplets. The reader is referred to these two papers as we will not repeat the formalism for the sake of space. Young's analysis is based on the Langmuir concept which devides the fluid field into three regions: the droplet itself, the thin Knudsen layer about the droplet where molecular transfer processes apply and the outer region governed by continuous heat and mass transfer. The fluxes of heat and mass in the different regions are matched at the interfaces. The analysis relies on the following definitions and assumptions:

- The gas/vapor volume including a single droplet is finite, adiabatic and of constant mass. Its boundary extends much further into the droplets surroundings than the droplets thermal and diffusive boundary layers. This situation allows the use of quasi-steady-state equations with boundary conditions changing gradually according to an overall mass and heat balance (temperature T_∞ and vapor pressure p^{v}_∞).
- Droplets and boundary layers form a spherical system.
- The temperature T_{d} and the pressure $p^{\mathrm{l}}_{\mathrm{d}}$ are uniform throughout the droplet.
- The droplet is in thermodynamic equilibrium with the vapor right over its curved surface, i.e. the vapor pressure at the droplet surface is the equilibrium vapor pressure p_{e} corresponding to T_{d} and the curvature (see Kelvin equations below).
- In the outer region vapor mass is transferred to the droplet by Fick's diffusion. Pressure (total) and thermal diffusion are neglected. Heat is transferred away from the droplet by heat conduction only. The driving potentials for diffusion and conduction are small to allow for linearisations in the governing equations.
- Mass and thermal accommodation coefficients are set equal to one.

When the droplet is very small ($Kn \gg 1$) the flux densities in the continuum region diminish so much that molecular transfer controls the growth rate. In this case the model retains the Hertz–Knudsen formula. In the other limit ($Kn \ll 1$) the flux densities in the outer region dominate and control growth. The retained equations are referred to as Maxwell's equations. When the droplet grows through the transition regime bridging the two extremes the full model needs to be applied. This is demonstrated in Fig. 1 in the case of water droplets growing in nitrogen. The nuclei are born below 10^{-3} μm and Knudsen number one is passed at 0.05 μm. The Hertz–Knudsen formula holds for the first stage of growth overpredicting the experiment dramatically for $Kn < 1$. The Maxwell equations overshoot at the beginning where they do not apply. This results in a remaining upward shift of the further growth curve. Only the full model covers the entire range of growth correctly.

In a binary system one starts out with a more complex phase equilibrium at a flat surface (Fig. 2). When the two species are similar with respect to the molecular forces of interaction the mixture is called ideal and the vapor pressures $p_{i,s}$ of the species as well as their sum are proportional to the liquid composition

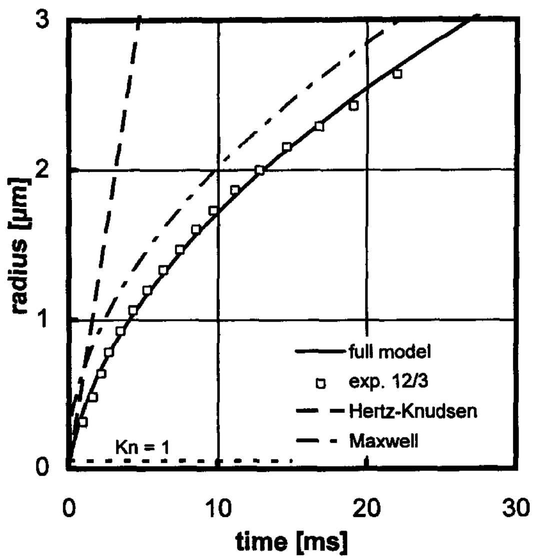

Fig. 1. Growth calculations in comparison applied to water droplets growing in nitrogen: the Hertz–Knudsen formula, Maxwell's equations and the full model according to Young [19, 1].

x_i (Raoult's law). This is expressed through equation (1)

$$p_{i,s}(x_i, T) = x_i\gamma_i(x_i, T)p_{i,0}(T) \tag{1}$$

when the activity coefficients γ_i are unity. The $p_{i,0}$ are the equilibrium vapor pressures of the pure components. Activity coefficients different from one denote deviation from ideality. They can be determined by different models. For our very non-ideal system we use the van Laar equations (Appendix). Figure 2 shows the resulting y vs x curve at fixed temperature. Our non-ideal system has an azeotrope ($y = x$) coinciding with an extremum of the total pressure.

The thermodynamic equilibrium at the binary droplet's surface does not only depend on the droplet temperature T_{d} and the composition x, but also on the droplet radius r_{d} (when r_{d} is very small). The partial equilibrium vapor pressure $p_{i,e}$ of such a droplet is given by the Kelvin equations [20]

$$p_{i,e}(r_{\mathrm{d}}, x, T_{\mathrm{d}}) = p_{i,s}(x, T_{\mathrm{d}}) \exp\left(\frac{2\sigma(x, T_{\mathrm{d}})v_i^l(x, T_{\mathrm{d}})}{\hat{R}T_{\mathrm{d}}r_{\mathrm{d}}}\right). \tag{2}$$

Here $\hat{R}$ is the gas constant, σ is the surface tension of the mixed droplet and v_i^{l} is the partial molar volume of species i in the liquid.

Incorporating the binary phase equilibrium we found it possible to extend Young's model to binary droplet growth under the additional assumptions:

- The binary droplet is homogeneously mixed, i.e. internal diffusion due to surface enrichment is too slow a process.

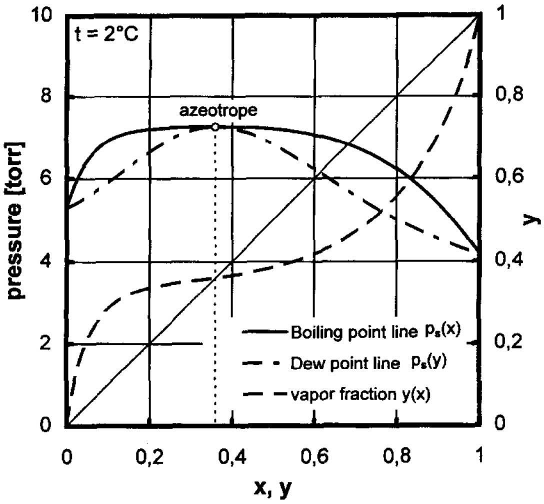

Fig. 2. Phase equilibrium of the binary system water-*n*-propanol at 2°C showing the boiling point line, the dew point line and the vapor mole fraction y as function of the liquid mole fraction x.

- The vapor diffusion process is considered as being composed of two independent diffusion streams adding up to the total mass flux. This means basically a two-fold application of the formalism of the single vapor case. The driving potential for each stream is the pressure difference between the outer boundary and the surface. The partial vapor pressures on the surface depend now on droplet temperature, radius *and composition.*

As in the unary case [1] a few simplifications are introduced justified by our experimental conditions. The ratios of both T_∞/T_d and T_∞/T_int are of order unity since small temperature differences are assumed. The ratios $p^\mathrm{v}_{i,\mathrm{int}}/p$ are substituted by $p^\mathrm{v}_{i,\infty}/p$ since small differences between partial vapor pressures at the interface $p^\mathrm{v}_{i,\mathrm{int}}$ and in the far field $p^\mathrm{v}_{i,\infty}$ are assumed.

The ratio $r_\mathrm{d}/r_\mathrm{int}$ varies between zero in the molecule limit ($Kn \to \infty$) and one in the continuum limit ($Kn \to 0$) (note that subscripts are confused in Ref. [1]). We keep it equal to one in the first term of the denominator (equation (3) and (8) of Ref. [1]) and equal to zero in the second term. This can be done because the second term diminishes anyway when $Kn \to 0$ and dominates when $Kn \to \infty$. Furthermore we omit the last term of Young's equation (43) [19] (note that this equation (43) is misprinted as (59) in Ref. [1]). This is allowed whenever this term is numerically insignificant which is the case in our calculations. In total these simplifications eliminate the Knudsen layer quantities $p^\mathrm{v}_\mathrm{int}$, T_int and r_int, substantially reducing the original system of equations.

We can now rewrite Young's equations for the mass and heat flux density in the binary case

$$J^\mathrm{m}_i = \frac{D_i p}{R_i T_\infty r_\mathrm{d}\left(1+4\sqrt{\dfrac{\bar{R}}{R_i}\dfrac{Kn}{Sc_i}}\dfrac{p}{p_{3,\infty}}\right)}\,\frac{p_{i,e}-p^\mathrm{v}_{i,\infty}}{p_{3,\infty}} \tag{3}$$

$$J^\mathrm{q} = \frac{\bar{k}(T_\mathrm{d}-T_\infty)}{r_\mathrm{d}\left(1+\dfrac{8Kn}{\Gamma Pr}\dfrac{\bar{\kappa}}{\bar{\kappa}-1}\right)} \tag{4}$$

where

$$\Gamma = \sum_i y_i \frac{\kappa_i+1}{\kappa_i-1}\sqrt{\frac{R_i}{\bar{R}}}. \tag{5}$$

There are two mass fluxes of the condensable vapors ($i = 1,2$ in equation (3)) and one heat flux (equation (4)). The sum in equation (5) has three terms ($i = 1,2,3$) including the carrier gas. Equations (3) and (4) involve the following definitions for the Knudsen, the Schmidt and the Prandtl number

$$Kn = \frac{\bar{\lambda}}{2r_\mathrm{d}};\quad Sc_i = \frac{\bar{\eta}}{\bar{\rho}D_i};\quad Pr = \frac{\bar{\eta}\bar{c}_\mathrm{p}}{\bar{k}}. \tag{6}$$

The required properties of the vapor/gas mixture are the specific gas constant $\bar{R}$, the ratio of specific heats $\bar{\kappa}$, the mean free path $\bar{\lambda}$, the viscosity $\bar{\eta}$, the density $\bar{\rho}$, the specific heat capacity $\bar{c}_\mathrm{p}$, the thermal conductivity $\bar{k}$ and the diffusion coefficient D_i. These are mean values depending on mixture composition, temperature and pressure. Appropriate mixing rules have been used for their evaluation given in the Appendix.

The mass flux $\Sigma_i J^\mathrm{m}_i$ condensing on the droplet surface causes a heat flux J^q into the gas and an internal heat flow into the droplet due to latent heat release. Gyarmathy [2] showed that temperature differences inside the droplet have to be taken into account only for very rapid change of boundary conditions like the passage of a shock wave. The heat of mixing can also be neglected because it is small compared to the latent heat release. Therefore, equations (3) and (4) are linked as follows

$$J^\mathrm{q} = -\sum_i L_{i,0}(T_\mathrm{d})J^\mathrm{m}_i \tag{7}$$

with the latent heat $L_{i,0}$ of the pure components given in the Appendix.

Inserting equation (3) and (4) into equation (7) we get one equation for the remaining unknowns T_d and r_d. The missing relation is the continuity equation

$$\sum_i J^\mathrm{m}_i = -\rho^\mathrm{l}(x, T_\mathrm{d})\frac{\mathrm{d}r_\mathrm{d}}{\mathrm{d}t} \tag{8}$$

where ρ^l is the liquid density belonging to droplet temperature and composition.

3. EXPERIMENTAL

3.1. *Droplet generation and growth*

In this investigation we utilize homogeneous binary nucleation for the generation of monodisperse droplets evenly distributed in space. We skip a discussion of the binary nucleation itself referring to recent theoretical and experimental work [18, 21–23] and proceed to the essentials of the generation mechanism.

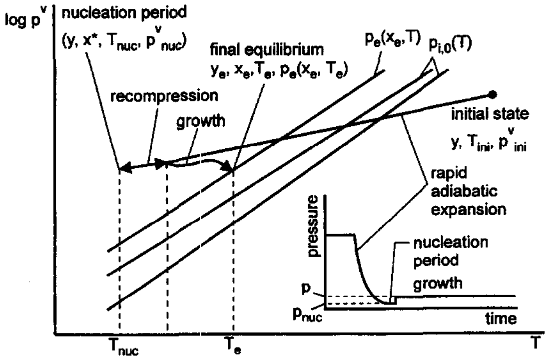

Fig. 3. Droplet generation and growth by means of the pex-tube process.

Figure 3 illustrates the process of droplet generation and growth by means of the pex-tube in a p-T-diagram. The binary vapor mixture diluted in carrier (initial state) is subjected to a transient expansion–compression process yielding a short nucleation period. During this period of supersaturated state T_{nuc} and $p^v{}_{nuc}$ a finite number of nuclei is born at the critical size r_d^* with interior composition x^*. According to the classical nucleation theory r_d^* and x^* can be calculated by solving the Kelvin equations (2). With known critical size and composition the rate J at which nuclei are born is then given by

$$J = C \cdot \exp\left(\frac{-4\pi r_d^{*2}\sigma(x^*)}{3k_B T_{nuc}}\right). \quad (9)$$

The kinetic factor C depends on temperature and vapor pressures of the gaseous phase and on size and composition of the critical nuclei. Thus a supersaturated state with fixed T_{nuc} and $p^v_{i,nuc}$ corresponds to a certain nucleation rate. Nucleation experiments [18] have been performed with various nucleation rates ranging from 10^5 to 10^9 cm^{-3}s^{-1} corresponding to droplet number concentrations between 50 and $5 \cdot 10^5$ cm^{-3}.

After the nucleation period a slight elevation of pressure and temperature inhibits further nucleation. Yet, supersaturation is maintained so that droplet growth is observed right after the nucleation period. Number concentration and growth of the condensing droplets are detected optically by means of a Mie light scattering technique providing radius vs time plots.

In principle growth continues until final equilibrium is reached with droplet composition x_e, uniform temperature $T_d = T_\infty = T_e$ and pressures $p^v_{i,\infty} = p_{i,e}(x_e, T_e)$. In practice observation time is limited due to heat release from the tube walls which may influence droplet growth. During observation time in the present experiments ($\leqslant 50$ ms) this effect is assessed to be negligible.

3.2. *Experimental set-up*

A sketch of the experimental set-up is shown in Fig. 4. Details about the idea and operation of the piston-expansion-tube (pex-tube) are published elsewhere [17, 18]. Here we confine ourselves to a brief description. The pex-tube consists basically of expansion tube (70 mm dia.) and driver tube (100 mm dia.), buffer tank, filling bulbs, vacuum pump and connecting lines. Except for the driver unit all parts form a closed system. In order to obtain well defined initial conditions, the expansion tube, the tank and the connecting lines are electrically heated to equal temperatures checked by PT-100 sensors. The whole system is evacuated prior to filling with the vapor mixture. The filling bulbs contain the liquids of the pure components in equilibrium with their vapors. The vapors and the carrier gas enter the system one after the other at desired partial pressures while thorough mixing is assured. The partial pressures are determined by an absolute pressure transducer (MKS

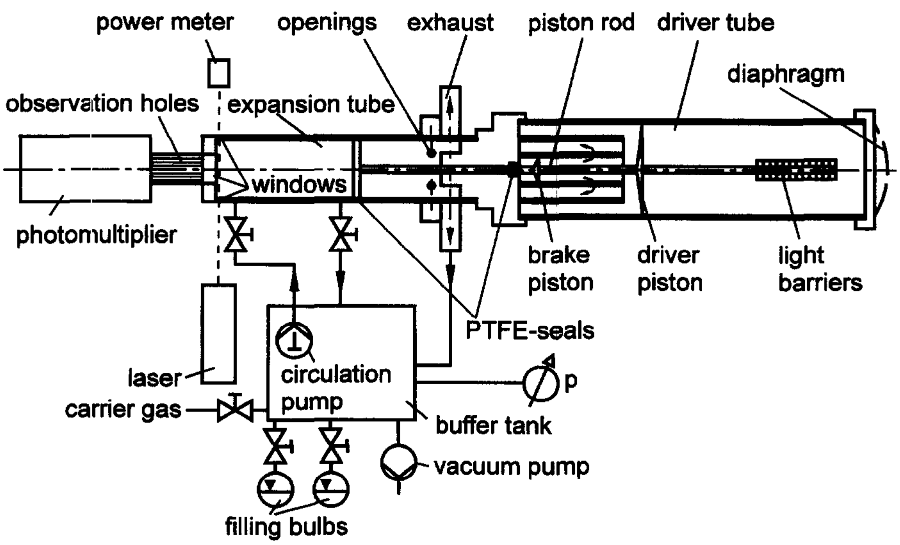

Fig. 4. Sketch of the experimental set-up.

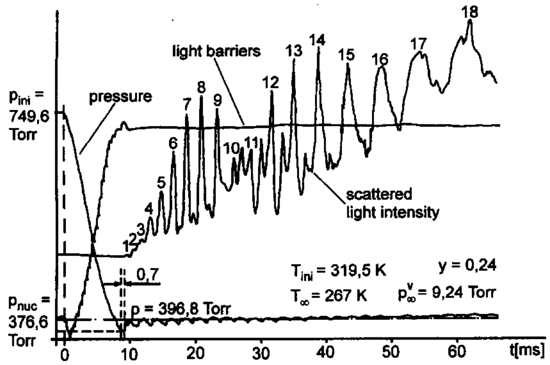

Fig. 5. Typical measuring run showing traces of total pressure, piston displacement and scattered light intensity.

Baratron 390H) with a measuring range from 10^{-3} to 10^3 Torr.

The expansion tube is confined by the observation window at one end and the expansion piston at the opposite end. It is separated from the rest of the system by valves. Displacement of the piston enlarges the volume of the expansion tube entailing rapid adiabatic expansion of the enclosed gas. The pressure at the end-wall is monitored by means of an acceleration compensated pressure transducer (Kistler 6031). The piston displacement is measured by an array of light barriers located in the driver tube. When the piston approaches the opposite wall it undergoes abrupt stopping. The expansion ceases and a small compression wave builds up travelling backwards into the expanded gas. The turn from expansion to compression gives rise to a small period of lowest pressure—the nucleation period. By tuning the stopping rate the nucleation period takes an appropriate length of typically 0.7 ms. The acceleration and breaking of the piston is achieved by the combination of driver and brake piston in the driver tube.

Droplet growth is observed close to the window where the condensing droplets are at rest. A 90° light scattering system is set up using an argon–ion laser (514.5 nm) and a calibrated photomultiplier. The scattering angle is fixed by an array of 25 narrow channels corresponding to a total sensitive volume of 91.2 mm^3. Size and number concentration of the droplets can be determined independently as function of time from the scattered light intensity.

3.3. *Measuring run*

An example of a typical measuring run is given in Fig. 5 presenting signals of pressure, piston displacement and scattered light intensity as function of time. The pressure starts at a constant level ($p_{\mathrm{ini}} \approx 750$ Torr) followed by an expansion of 8.5 ms which ends in the nucleation period ($p_{\mathrm{nuc}} \approx 377$ Torr). The piston displacement appears as a step function, each step corresponding to a certain position, i.e. volume. By measuring volume and pressure in combination with gasdynamic calculations we have assured that the dry tube expansion is isentropic. The nucleation temperature T_{nuc} is thus found from Poisson's law

$$T_{\mathrm{nuc}} = T_{\mathrm{ini}}\left(\frac{p_{\mathrm{nuc}}}{p_{\mathrm{ini}}}\right)^{\frac{\bar{\kappa}-1}{\bar{\kappa}}} \tag{10}$$

where T_{ini} is the initial temperature before expansion. The nucleation temperature $T_{\mathrm{nuc}} \approx 263$ K is kept constant in all experiments. The ratio of specific heats $\bar{\kappa}$ of the gas/vapor mixture is determined at the actual mixture's composition and at the mean temperature between the initial and the nucleation state.

The recompression elevates the total pressure from p_{nuc} to p by approximately 20 Torr. This corresponds to an increase in temperature from T_{nuc} to T_∞ of about 3.5 K. At the beginning of droplet growth we have the partial vapor pressures $p^{\mathrm{v}}_{\mathrm{i},\infty}$.

The intensity of the scattered light starts to rise right after the nucleation period. In the course of time it exhibits the resonances of a Mie signal (peaks are numbered). The signal corresponds to diameter and number concentration of the scattering droplets as described in Ref. [1]. The signal evaluation relies on the refractive index which needs further consideration.

The refractive index $n_{i,0}$ of a pure substance depends on the liquid temperature and the wavelength of light. The refractive indices of the substances investigated are not reported in the literature for the actual temperature range and wavelength of the laser. Therefore, we measured the refractive indices of pure *n*-propanol and water at various temperatures at 514.5 nm [18]. Results are listed in the Appendix as best polynomial fits.

The droplets consist of a liquid mixture the composition of which is not measured. Most likely concentration gradients are established inside the droplet due to surface enrichment of *n*-propanol. Furthermore calculations of the droplet growth show that the droplet temperature depends on the mixture composition. Thus, in principle we are dealing with an unknown refractive index of the droplets. The uncertainty is comparatively small for small droplet sizes. Calculations of the first peak with the refractive indices of the pure substances predict only slight differences for droplet size and scattered intensity, but uncertainty is increasing with increasing droplet diameter leading to remarkable errors in the detection of droplet size. Therefore, we determined a refractive index for each experiment corresponding to the mean droplet composition using data by Chu and Thompson [24] (see Appendix).

4. RESULTS AND COMPARISON WITH MODEL

4.1. *Remarks on computation*

Radius vs time plots are computed from equations (3), (4), (7) and (8) numerically in time steps. The initial values for p, $p^{\mathrm{v}}_{\mathrm{i},\infty}$ and T_∞ are provided by the experiment. Growth calculation begins in the centre of the nucleation period from which the droplets ema-

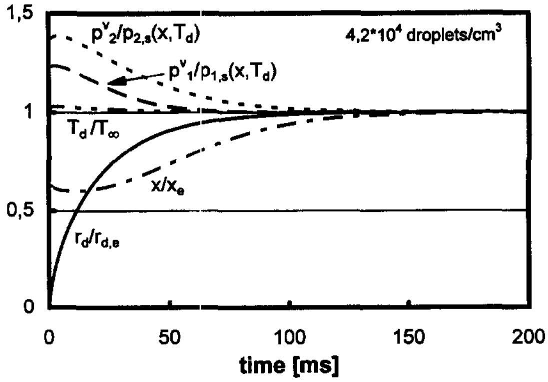

Fig. 6. Model calculation of partial vapor pressures $p^v_{i,\infty}$, droplet radius r_d and droplet composition x normalized with their equilibrium values. Note that $r_{d,e}$ is identified where $dr_d/dt = 0$. The droplet temperature T_d is normalized with the actual background temperature T_∞.

nate with the critical radius r_d^* and the critical composition x^* computed from Kelvin's equations (2). Since the critical droplet is in principle in equilibrium with its surroundings it needs an artificial first growth step. With that step a new temperature and composition is computed and so forth. The influence of the starting conditions decays totally after a few time steps. Time steps of 10 μs prove to be sufficiently short. During the growth process the composition x is a variable like the radius, the temperatures and the pressures. With vapor depletion and heat addition taken into account all these variables approach the droplet vapor equilibrium for a constant number of droplets. Figure 6 shows the computed curves under typical conditions.

For each time step all needed physical properties are recomputed depending on the actual temperatures, compositions and pressures in the liquid and the gas mixture according to sources referred to in the Appendix. Because we are dealing with small temperature gradients the temperature dependent properties of the vapor/carrier mixture are evaluated at the far field temperature T_∞.

4.2. *Results*

Experimental results on droplet growth in the water–n-propanol system are shown in Fig. 7. Each symbol represents a particular experiment and each data point corresponds to a peak of the scattered light signal. The solid lines are the results of the model calculations. The origin of the time axis is placed in the centre of the nucleation pulse. Initial temperature and total pressure of the vapor/carrier mixture ($T_\infty \approx 266.5$ K, $p \approx 395$ Torr) are the same for each experiment. The droplet number concentration is roughly 1500 cm^{-3} in all experiments. At this number concentration the calculations reveal that vapor depletion and latent heat release are hardly noticeable within the observation time. In such a case substantial computing time is saved by simply taking the physical properties to be constant. Figure 7 splits into (a) and

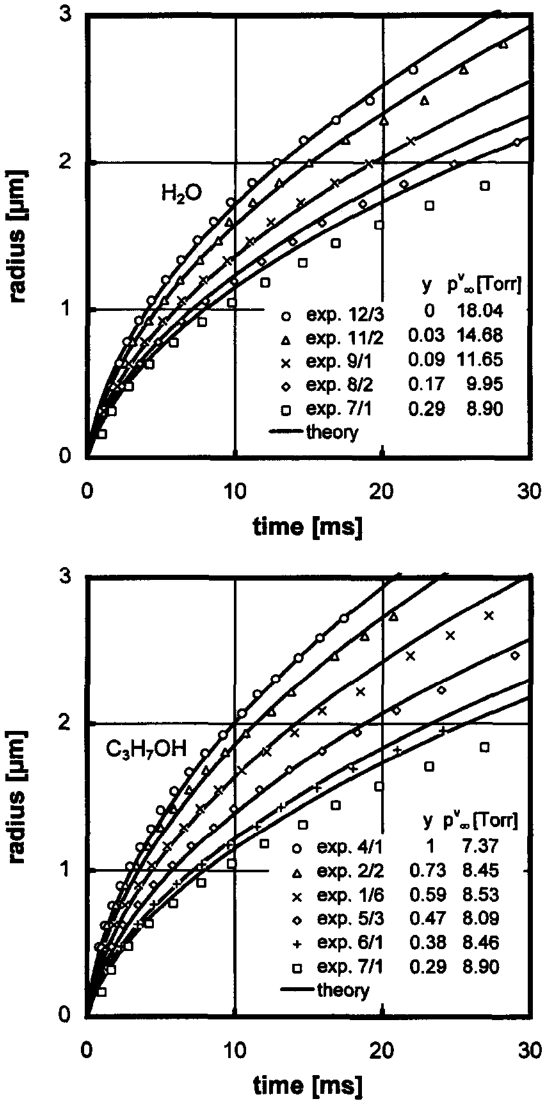

Fig. 7. Growth curves for water-n-propanol droplets suspended in nitrogen. y is the mole fraction of n-propanol in the vapor, p^v_∞ is the total vapor pressure at the beginning of growth. Symbols represent experiments, solid lines are model calculations. The average droplet number concentration is 1500 cm^{-3} and the initial growth temperature is 266.5 K for each experiment.

(b). We start with pure water in the first graph (top curve) and by increasing y step down to the bottom curve representing the slowest growth. This curve is copied over to 7(b) and with further increase of y we now step up to the pure n-propanol curve (top). Considering the approximations made and the extent of physical properties entering our model provides very satisfying agreement with the experimental data except for the bottom curve. We could not find any clue as to the poor prediction of this curve.

In this set of curves one wants to keep everything constant except y to study the effect of composition. This is not entirely achievable because the request of a constant number concentration (nucleation rate) entails a variation of the total vapor pressure p^v_∞,

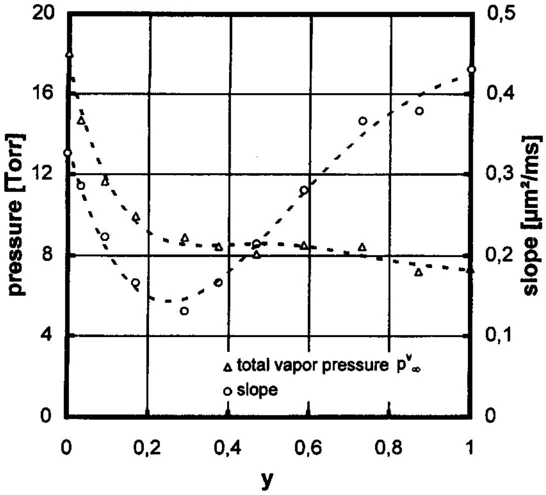

Fig. 8. Total vapor pressure p^v_∞ and slope for experiments shown in Fig. 7 as function of n-propanol vapor fraction y.

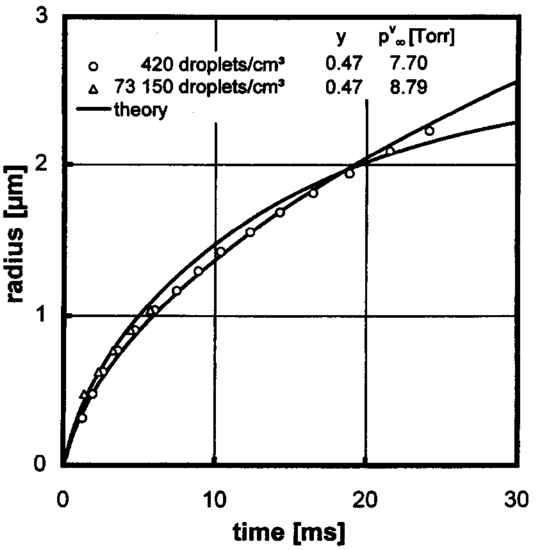

Fig. 9. Effect of number concentration on droplet growth.

especially on the water rich side (see legend of Fig. 7). Figure 8 attempts to interpret the influence of y using the data of Fig. 7 plus one additional experiment for $y = 0.87$. First the total pressure p^v_∞ is shown as it drops down from the water side to a fairly constant level for $y > 0.2$. Second the individual growth curves of Fig. 7 are represented by their slope dr_d^2/dt. This slope is almost a constant number for each curve since most of the growth takes place in the continuum regime where the growth model merges with a quadratic law. We observe, at least for $y > 0.2$, how the growth rate (slope) depends solely on the composition. The smallest slope seems to coincide with the azeotropic y (see Fig. 2). This can be rationalized by the fact that the total vapor pressure has its maximum in the azeotropic point which means a minimum in driving potential.

As mentioned the experiments of Fig. 7 are hardly affected by vapor depletion and latent heat release. They become noticeable with higher number concentrations as illustrated in Fig. 9. Temperature and composition are the same in both experiments shown. The difference in number concentration is two orders of magnitude. We see that the higher number concentration makes growth faster in the beginning which is due to the corresponding higher total vapor pressure. In the further course the growth rate reduces strongly due to vapor depletion. The number of data points on this curve is limited because the light intensity exceeds the range of the photomultiplier.

5. CONCLUSIONS

On the basis of previous work on the growth of unary droplets we have carried out experiments on binary, monodisperse droplets composed of water and n-propanol. The droplets were generated by binary nucleation in a pex-tube and observed by light scattering up to a few μm. The entire mixing range from pure water to pure n-propanol was covered. It appeared that the mixed droplet grows slower than the pure one with a minimum around the azeotropic point. This suggests that droplets in a system with a maximum-boiling azeotrope (i.e. a minimum in the p-x-curve) should grow faster than the pure ones.

We interpreted the experimental results successfully using the following concept. The condensing binary vapor is considered as two unary streams each driven by its own pressure gradient. The streams determine the droplet composition which in turn affects the pressure gradients until a final equilibrium is reached. One flux of released latent heat is transferred away from the droplet through the vapor/carrier mixture. This concept allows the extension of a formerly approved unary model to the binary problem. In doing so it proved to be very important to evaluate precise physical properties as they depend on vapor and liquid composition.

Acknowledgments—This work was supported by grant no. Pe 401/7 of Deutsche Forschungsgemeinschaft (DFG).

REFERENCES

1. Peters, F. and Paikert, B. Measurement and interpretation of growth and evaporation of monodispersed droplets in a shock tube. *International Journal of Heat and Mass Transfer*, 1994, **37**(2), 293–302.
2. Gyarmathy, G. The spherical droplet in gaseous carrier streams: review and synthesis. In *Multiphase Science and Technology*, Vol. 1 Hemisphere, Washington, 1982, pp. 99–279.
3. Mozurkewich, M. Aerosol growth and the condensation coefficient for water: a review. *Aerosol Science and Technology*, 1986, **5**, 223–236.
4. Barrett, J. C. and Clement, C. F. Kinetic evaporation and condensation rates and their coefficients. *Journal of Colloid Interface Science*, 1992, **150**(2), 352–362.
5. Kulmala, M. Condensational growth and evaporation in the transition regime. *Aerosol Science and Technology*, 1993, **19**, 381–388.
6. Fukuta, N. and Walter, L. A. Kinetics of hydrometer

growth from a vapor–spherical model. *Journal of the Atmospheric Sciences*, 1970, **27,** 1160–1172.
7. Kaser, A. Verhalten von Dämpfen löslicher Zweistoffgemische bei Expansion in Überschalldüsen—Tropfenkoaleszenz in einer Potentialwirbelströmung. *ZAMM*, 1973, **53**, 39–56.
8. Kulmala, M., Vesala, T. and Wagner, P. E. An analytical expression for the rate of binary condensational particle growth: comparison with numerical results. *Journal of Aerosol Science*, 1992, **23**, 133–136.
9. Studzinski, W., Zahoransky, R. A., Wittig, S. L. K. and Barschdorf, D. Droplet formation and growth in condensing binary vapors. *International Journal of Heat and Mass Transfer*, 1984, **27**(3), 451–460.
10. Studzinski, W., Spiegel, G. H. and Zahoransky, R. A. Binary nucleation and condensation in associated vapors. *Journal of Chemical Physics*, 1986, **84**(7), 4008–4014.
11. Spiegel, G. H., Zahoransky, R. A. and Wittig, S. L. K. Homogeneous and heterogeneous condensation of nonideal binary vapor mixtures in shock tube expansion flow. In (ed. D. Bershader and R. Hanson) *Proceedings of the 15th International Symposium on Shock Waves and Shock Tubes*, Stanford, CA, 1986, pp. 775–781.
12. Studzinski, W., Zahoransky, R. A. and Wittig, S. L. K. Zur Beschreibung homogener unärer und binärer Kondensationsvorgänge. *Wärme- und Stoffübertragung*, 1983, **17**, 241–250.
13. Rudolf, R., Majerowicz, A., Kulmala, M., Vesala, T., Viisanen, Y. and Wagner, P. E. Kinetics of particle growth in supersaturated binary vapor mixtures. *Journal of Aerosol Science*, 1991, **22,** 51–54.
14. Barrett, J. C. and Clement, C. F. Growth rates for liquid drops. *Journal of Aerosol Science*, 1988, **19**(2), 223–244.
15. Kulmala, M. and Vesala, T. Condensation in the continuum regime. *Journal of Aerosol Science*, 1991, **22**(3), 337–346.
16. Wagner, P. E. Aerosol growth by condensation. In *Aerosol Microphysics*, Vol. 2, ed. W. H. Marlow. Springer, Berlin, 1982, p. 129–178.
17. Peters, F. and Meyer, K. A. J. Measurement and interpretation of growth of monodispersed water droplets suspended in pure water. *International Journal of Heat and Mass Transfer*, 1995, **38**(17), 3285–3293.
18. Rodemann, T. and Peters, F. Experimental investigation of binary nucleation rates of water–*n*-propanol and water–*n*-butanol vapors by means of a pex-tube. *Journal of Chemical Physics*, 1996, **105**(12), 5168–5176.
19. Young, J. B. The condensation and evaporation of liquid droplets at arbitrary Knudsen number in the presence of an inert gas. *International Journal of Heat and Mass Transfer*, 1993, **36**(11), 2941–2956.
20. Neumann, K. and Döring, W. Tröpfchenbildung in übersättigten Dampfgemischen zweier vollständig mischbarer Flüssigkeiten. *Zeitschrift für Physikalische Chemie*, 1940, **A 186,** 203–226.
21. Wilemski, G. and Wyslouzil, B. E. Binary nucleation kinetics. I. Self-consistent size distribution. *Journal of Chemical Physics*, 1995, **103**(3), 1127–1136.
22. Kalikmanov, V. I. and van Dongen, M. E. H. Semi-Phenomenological kinetic theory of binary nucleation. *Europhysics Letters*, 1995, **29**(2), 129–134.
23. Viisanen, Y., Strey, R., Laaksonen, A. and Kulmula, M. Measurement of the molecular content of binary nuclei. II. Use of the nucleation rate surface for water-ethanol. *Journal of Chemical Physics*, 1994, **100**(8), 6062–6072.
24. Chu, K.-Y. and Thompson, A. R. Densities and refractive indices of alcohol-water solutions. *Journal of Chemical Engineering Data*, 1962, **3,** 358–360.
25. Strey, R., Wagner, P. E. and Viisanen, Y. Homogeneous nucleation rates of particle formation from vapor mixtures. In *Proceedings of 13th International Conference on Nucleation and Atmospheric Aerosols*, eds N. Fukuta and P. E. Wagner, Hampton, 1992, pp. 111–120.
26. Reid, R. C., Prausnitz, J. M. and Poling, B. E., *The Properties of Gases and Liquids*, 4th edn. McGraw Hill, New York, 1987.
27. Marrero, T. R. and Mason, E. A., Gaseous diffusion coefficients. *Journal of Physical and Chemical Reference Data*, 1972, **1**(1), 3–34.
28. Landolt–Börnstein. Stoffwerte und mechanisches Verhalten von Nichtmetallen. *Zahlenwerte und Funktionen aus Physik, Chemie, Astronomie, Geophysik und Technik*, vol 4, 6th edn. Springer, Berlin, 1955.
29. *VDI-Wärmeatlas*, 6th edn, Düsseldorf, 1991.
30. Sonntag, D. and Heinze, D., *Sättigungsdampfdruck- und Sättingungsdampfdichtetafeln für Wasser und Eis*. VEB Deutscher Verlag für Grundstoffindustrie, Leipzig, 1982.
31. Schmeling, T. and Strey, R., Equilibrium vapor pressure measurements for the *n*-alcohols in the temperature range from −30°C and +30°C. *Berichte der Bunsen-Gesellschaft für Physikalische Chemie*, 1983, **87,** 871–874.
32. Pruppacher, H. R. and Klett, J. D., *Microphysics of Clouds and Precipitation*. D. Reidel, Dordrecht, 1980.
33. Yen, L. C. and Woods, S. S., A generalized equation for computer calculation of liquid densities. *AIChE Journal*, 1966, **12**(1), 95–99.
34. Strey, R. and Schmeling, T., Surface tension measurements for the *n*-alcohols in the temperature range from −40°C and +40°C. *Berichte der Bunsen-Gesellschaft für Physikalische Chemie*, 1983, **87**, 324–327.

APPENDIX. PHYSICAL PROPERTIES

Liquid mixture's density

The density of the liquid mixture ρ^l is calculated assuming a linear relationship between the pure liquid densities $\rho^l_{i,0}$ from Table A2 and the mass fraction X_i of component i in the liquid droplet

$$\rho^l(X_i, T) = \sum_i X_i \rho^l_{i,0}(T).$$

Partial liquid volume

The partial molar volume v^l_i of species i in the liquid mixture is calculated according to

$$v^l_i(x_i, T) = v^l(x_i, T) + (1 - x_i)\frac{\partial}{\partial x_i} v^l(x_i, T).$$

The mean molar volume v^l of the liquid mixture can be evaluated by means of the liquid density ρ^l expressed in terms of the molar fraction x_i

$$v^l(x_i, T) = \frac{\Sigma_i x_i M_i}{\rho^l(x_i, T)}.$$

Liquid activity coefficients

Calculating the partial equilibrium vapor pressures $p_{i,s}$ according to equation (1) requires the knowledge of the activity coefficients γ_i. The activity constants are depending on temperature and mixture composition. The van Laar equations relate the activity coefficients to the composition of a binary mixture for a given temperature

$$\ln \gamma_1(x) = \frac{A}{\left(1 + \frac{A}{B}\frac{1-x}{x}\right)^2} \quad \ln \gamma_2(x) = \frac{B}{\left(1 + \frac{B}{A}\frac{x}{1-x}\right)^2}.$$

A and B are the van Laar constants. Strey *et al.* [25] fitted the constants to equilibrium vapor pressure measurements at 260 K. They found

$$A = 1.313 \quad B = 2.365.$$

Table A1. Thermodynamic properties of the pure gaseous components water, n-propanol and nitrogen

	M_i [kg/kmol]	Viscosity η_i [Pa/s]
Water	18.0152	$(1.823\cdot 10^{-6}\sqrt{T})/(1+673/T)$ [a]
n-Propanol	60.0956	$-1.42907\cdot 10^{-6}+1.45108\cdot 10^{-7}\sqrt{T}+2.26049\cdot 10^{-8}\cdot T$ [b]
Nitrogen	28.0134	$(1.378\cdot 10^{-6}\sqrt{T})/(1+103/T)$ [a]
	Specific heat capacity c_{pi} [J/kg K]	
Water	$1.25342\cdot 10^3+7.6775\cdot T-0.03345\cdot T^2+4.9728\cdot 10^{-5}\cdot T^3$ [b]	
n-Propanol	$-1.94022\cdot 10^3+2.31831\cdot 10^2\sqrt{T}-1.7757\cdot T-4.76687\cdot 10^{-4}\cdot T^2+1.42444\cdot 10^{-7}\cdot T^3$ [b]	
Nitrogen	1038	
	Thermal conductivity k_i [W/m K]	
Water	$7.341\cdot 10^{-3}-1.013\cdot 10^{-5}\cdot T+1.801\cdot 10^{-7}T^2-9.1\cdot 10^{-11}\cdot T^3$ [c]	
n-Propanol	$-7.931\cdot 10^{-3}+3.987\cdot 10^{-5}\cdot T+1.193\cdot 10^{-7}T^2-5.021\cdot 10^{-11}\cdot T^3$ [c]	
Nitrogen	$3.919\cdot 10^{-4}+9.816\cdot 10^{-5}\cdot T-5.067\cdot 10^{-8}T^2+1.504\cdot 10^{-11}\cdot T^3$ [c]	

[a] Landolt-Börnstein [28].
[b] Best fit of data from VDI-Wärmeatlas [29].
[c] Reid *et al.* [26].

Since droplet growth takes place at higher temperatures we use a temperature correction known as the regular solution [26]

$$\gamma_i(x,T)=\gamma_i(x)^{\frac{T_0}{T}}$$

where T_0 is the reference temperature.

Binary surface tension

The surface tension data of the mixture exist at particular temperatures, e.g. at 260 K [25], but not at the varying growth temperatures. We use, therefore, the generalized, temperature dependent equation of Tamura *et al.* as reported in Ref. [26].

$$\sigma(x_i,T)=\left(\sum_i \psi_i^\sigma(x_i,T)\sigma_{i,0}(T)^{0.25}\right)^4.$$

Solving the following equations yields ψ^σ_i the superficial volume fraction of component i in the surface layer.

$$\log\left(\frac{\psi_i^\sigma(x_i,T)^q}{1-\psi_i^\sigma(x_i,T)}\right)=\log\left(\frac{\psi_i(x_i,T)^q}{1-\psi_i(x_i,T)}\right)+W(T)$$

with

$$W(T)=0.441\frac{q}{T}\left(\frac{\sigma_{2,0}(T)v^{\rm l}_{2,0}(T)^{2/3}}{q}-\sigma_{1,0}(T)v^{\rm l}_{1,0}(T)^{2/3}\right)$$

and

$$\psi_i(x_i,T)=\frac{x_i v^{\rm l}_{i,0}(T)}{\Sigma_i x_i v^{\rm l}_{i,0}(T)}$$

ψ_i is the volume fraction in the bulk liquid, where $v^{\rm l}_{i,0}=M_i/\rho^{\rm l}_{i,0}$ is the molar volume of the pure component i. The densities $\rho^{\rm l}_{i,0}$ and the surface tensions $\sigma_{i,0}$ of the pure components are from Table A2. The constant q depends on type and size of the organic constituent. In the case of alcohols q identifies the number of carbon atoms. The surface tension is obtained in mN/m, when $v^{\rm l}_{i,0}$ is inserted in cm^3/mol and $\sigma_{i,0}$ in mN/m.

The influence of the surface tension on growth is rather weak. It enters equation (2) where it affects the partial equilibrium vapor pressures only for very small radii.

Mixture's refractive index

To determine the refractive index n of the mixed droplet we refer to data obtained by Chu and Thompson [24] at

Table A2. Thermodynamic properties of the pure liquid components water and n-propanol

	Saturation vapor pressure $p_{i,0}$ [Pa]	
Water	$\exp\left(21.125-0.0272455\cdot T+1.68534\cdot 10^{-5}\cdot T^2+2.45755\cdot\ln(T)-\frac{6094.4642}{T}\right)$ [a]	
n-Propanol	$133.32\cdot\exp\left(-\frac{11286.4904}{T}+150.24797-19.19\cdot\ln(T)\right)$ [b]	
	Density $\rho^{\rm l}_{i,0}$ [kg/m^3]	
Water	$999.84+0.086\cdot t-0.0108\cdot t^2$ [c]	
n-Propanol	$0.2744(1+1.85051\cdot\tau^{1/3}+0.82572\cdot\tau^{2/3}+0.10428\cdot\tau^{4/3})$ with $\tau=1-T/536.8$ K [d]	
	Surface tension $\sigma_{i,0}$ [N/m]	Refractive index $n_{i,0}$ (514.5 nm)
Water	$0.0761-1.55\cdot 10^{-4}\cdot t$ [c]	$1.33666-1.3265\cdot 10^{-5}\cdot t-1.7027\cdot 10^{-6}\cdot t^2$ [e]
n-Propanol	$0.02528-8.394\cdot 10^{-5}\cdot t$ [f]	$1.39585-3.750\cdot 10^{-4}\cdot t$ [e]

[a] Sonntag and Heinze [30].
[b] Schmeling and Strey [31].
[c] Pruppacher and Klett [32].
[d] Yen and Woods [33].
[e] Rodemann and Peters [18].
[f] Strey and Schmeling [34].

20°C and a wavelength of 589 nm. The following polynom is a best fit to their data.

$$n(X) = 1.33359 + 0.09037 \cdot X - 0.03862 \cdot X^2.$$

Comparison with our measurements (Table A2) at the actual wavelength and temperature show that the difference between the pure substance refractive indices is smaller than 0.72% for n-propanol and 0.18% for water.

Latent heat

The latent heat $L_{i,0}$ of a pure component is inferred from the Clausius–Clapeyron equation

$$L_{i,0}(T) = \frac{R_i \cdot T^2}{p_{i,0}(T)} \frac{\mathrm{d}}{\mathrm{d}T} p_{i,0}(T)$$

with the specific gas constant R_i and the vapor pressures $p_{i,0}$ from Table A2.

Properties of the vapor–carrier gas mixture

The following properties of the vapor/carrier mixture are calculated assuming an ideal mixture with the ideal gas equation $p_i v_i = \bar{R}T$ and Daltons law $p_i = y_i p$ valid.

$$\bar{R} = \sum_i Y_i R_i, \quad \bar{c}_p = \sum_i Y_i c_{p_i}, \quad \bar{\rho} = \frac{p}{\bar{R}T}, \quad \bar{\kappa} = \frac{\bar{c}_p}{\bar{c}_p - \bar{R}}.$$

The gas mixture's viscosity $\bar{\eta}$ and thermal conductivity $\bar{k}$ are calculated according to Wilkes mixing rule [26]

$$\bar{\eta} = \sum_i \frac{y_i \eta_i}{\Sigma_j y_j \phi_{ij}} \quad \bar{k} = \sum_i \frac{y_i k_i}{\Sigma_j y_j \phi_{ij}}$$

with

$$\phi_{ij} = \frac{[1 + \sqrt{\eta_i/\eta_j} \cdot (M_j/M_i)^{1/4}]^2}{\sqrt{8(1 + M_i/M_j)}}.$$

From kinetic theory of gases the mean free path $\bar{\lambda}$ is related to the viscosity

$$\bar{\lambda} = \frac{\bar{\eta}}{2} \frac{\sqrt{2\pi \bar{R}T}}{p}.$$

The diffusion coefficients D_i are evaluated according to Blanc's law [27] assuming that substance i is a dilute component diffusing into a homogeneous mixture.

$$D_i = \left(\sum_{\substack{j \\ j \neq i}} \frac{y_j}{D_{ij}} \right)^{-1}.$$

Here D_{ij} are the binary diffusion coefficients, which are derived from Fuller's equation [26]. In the ternary mixture under investigation the subscript 1 denotes water, 2 n-propanol and 3 nitrogen. We get the following binary diffusion coefficients:

$$D_{12} = 4.78797 \cdot 10^{-3} \frac{T^{1.75}}{p}$$

$$D_{13} = 9.1546 \cdot 10^{-3} \frac{T^{1.75}}{p}$$

$$D_{23} = 3.74097 \cdot 10^{-3} \frac{T^{1.75}}{p}$$

where D_{ij} is in cm^2/s when p is inserted in Torr.